Supplementary Information

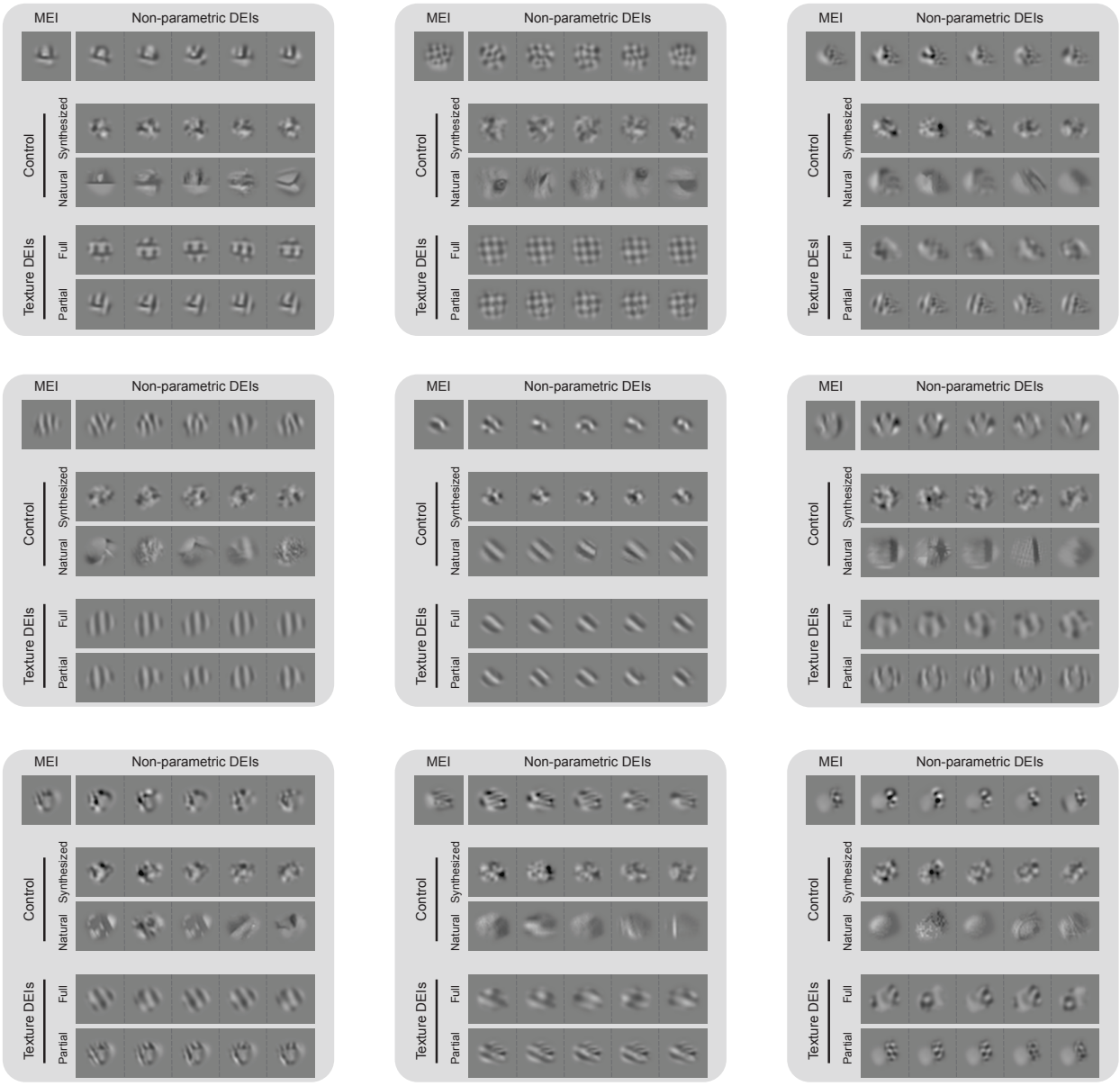

Fig. S1. Example stimuli presented in closed-loop experiments. MEI, non-parametric DEIs, natural & synthesized controls, and partial- & full-texture DEIs that were presented back to the animals in closed-loop experiments for 9 example neurons.

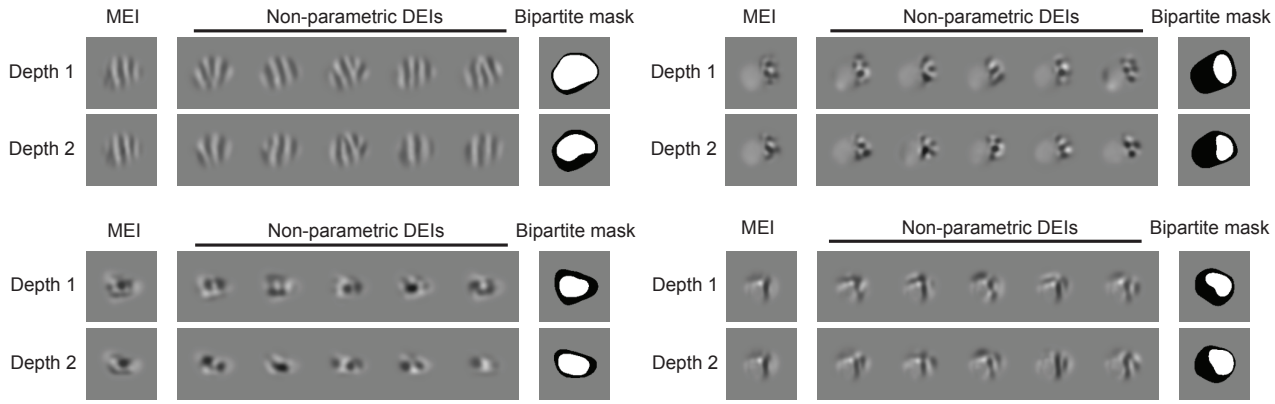

Fig. S2. MEI, DEIs, and bipartite mask of partial-texture DEIs generated from signals at different depths of the same neuron. Most neurons were scanned multiple times due to the dense calcium imaging with field 5μm apart in depths. MEI, DEIs, and partial-texture DEIs were generated for neuronal slices at different depths.

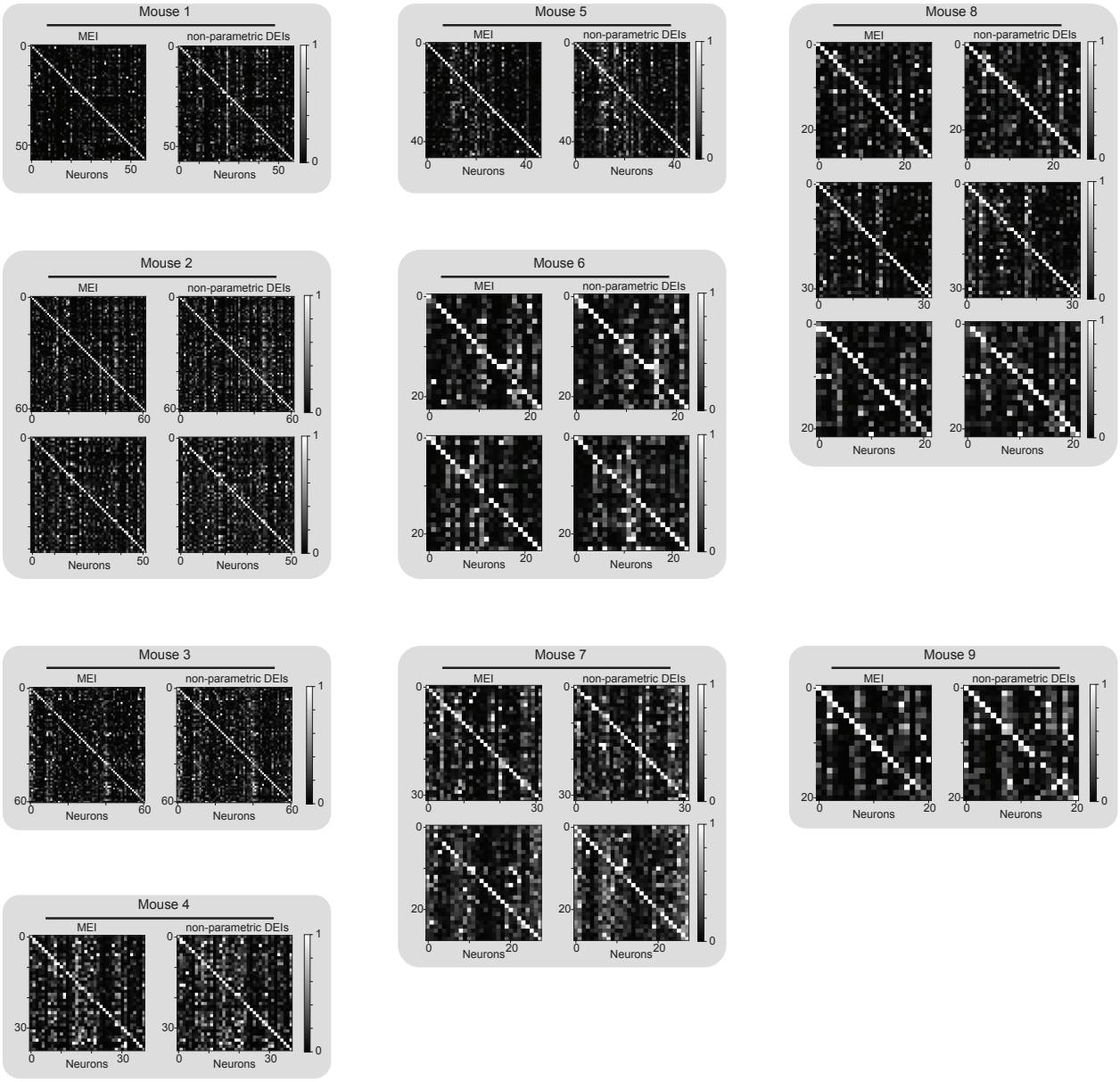

Fig. S3. MEI and DEIs activated neurons with high specificity in all mice. The confusion matrices show the responses of each neuron to the MEI (left) and DEIs (right) of all target neurons in individual scans where we presented the stimuli back to the mouse on day 2 and beyond in closed-loop experiments. MEI responses were averaged across 20 repeats of the same image while DEIs responses were averaged across 20 different images with single repeat. The responses of each neuron were normalized, and each row was scaled so the maximum response across all images equals 1. Responses of neurons to their own MEI and DEIs (along the diagonal) were larger than to other MEIs and DEIs, respectively (one-sided permutation test, $P < 10^{-9}$ for both cases across all mice).

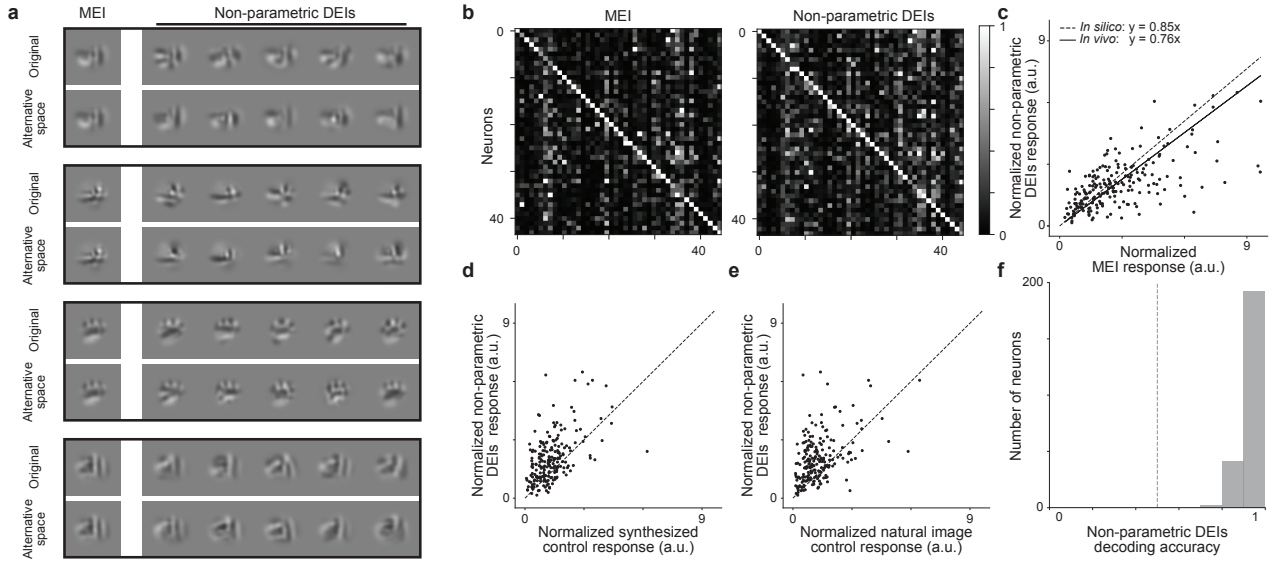

Fig. S4. Population-based DEIs evoked strong and selective responses in target neurons while containing perceivable differences. **a**, Examples of MEI and non-parametric DEIs generated with pixel-based (odd rows) or *in silico* population-based (even rows) diversity for 4 example neurons. **b**, Population-based DEIs activated neurons with high specificity. The confusion matrices show the responses of each neuron to MEI (left) and DEIs (right) of 44 neurons. MEI responses were averaged across 20 repeats of the same image while DEIs responses were averaged across 20 different images with single repeat. The responses of each neuron were normalized, and each row was scaled so the maximum response across all images equals 1. Responses of neurons to their own MEI and population-based DEIs (along the diagonal) were larger than to other MEIs and DEIs respectively (one-sided permutation test, $P < 10^{-9}$ for both cases). **c**, *In vivo* response to population-based DEIs versus MEI. Each point corresponds to the normalized response of a single neuron. The linear relationship between DEIs and MEI responses was estimated by averaging over 1000 repeats of robust linear regression using the RANSAC algorithm (21). DEIs stimulated *in vivo* closely to the level predicted *in silico* with respect to MEI (76% versus 85%) (two-sided Wilcoxon signed-rank test, $W = 8464$, $P = 7.69 \times 10^{-3}$), with only 12.1% of all neurons showing different responses between DEIs and 85% of MEI ($P < 0.05$, two-tailed Welch's t-test with 32.6 average d.f.). Data were pooled over 207 neurons from 5 mice. **d**-**e**, Each point corresponds to the normalized activity of a single neuron in response to its population-based DEIs versus its synthesized controls (**d**) or natural image (**e**) controls. Response to each stimulus type was averaged over 20 different images with single repeat. DEIs activated their target neurons stronger than their corresponding synthesized and natural image controls (one-sided Wilcoxon signed-rank test, $W = 3441$, $P < 10^{-9}$ and $W = 3466$, $P < 10^{-9}$ respectively) with 26.6% and 28.5% of all neurons showing greater responses to non-parametric DEIs ($P < 0.05$, one-tailed Welch's t-test with 31.0 and 30.6 average d.f., respectively). **f**, Differences between the most different pair of DEIs in pixel space are distinguishable by the mouse V1 population. Logistic regression classifiers were used to decode DEI identity of individual trials from V1 population responses. Decoding accuracies across neurons (median=0.93) were higher than chance level (0.5 as indicated by the dashed line) (one sample t-test, $t = 138.5$, $P < 10^{-9}$). Data were pooled over 235 neurons from 3 mice.

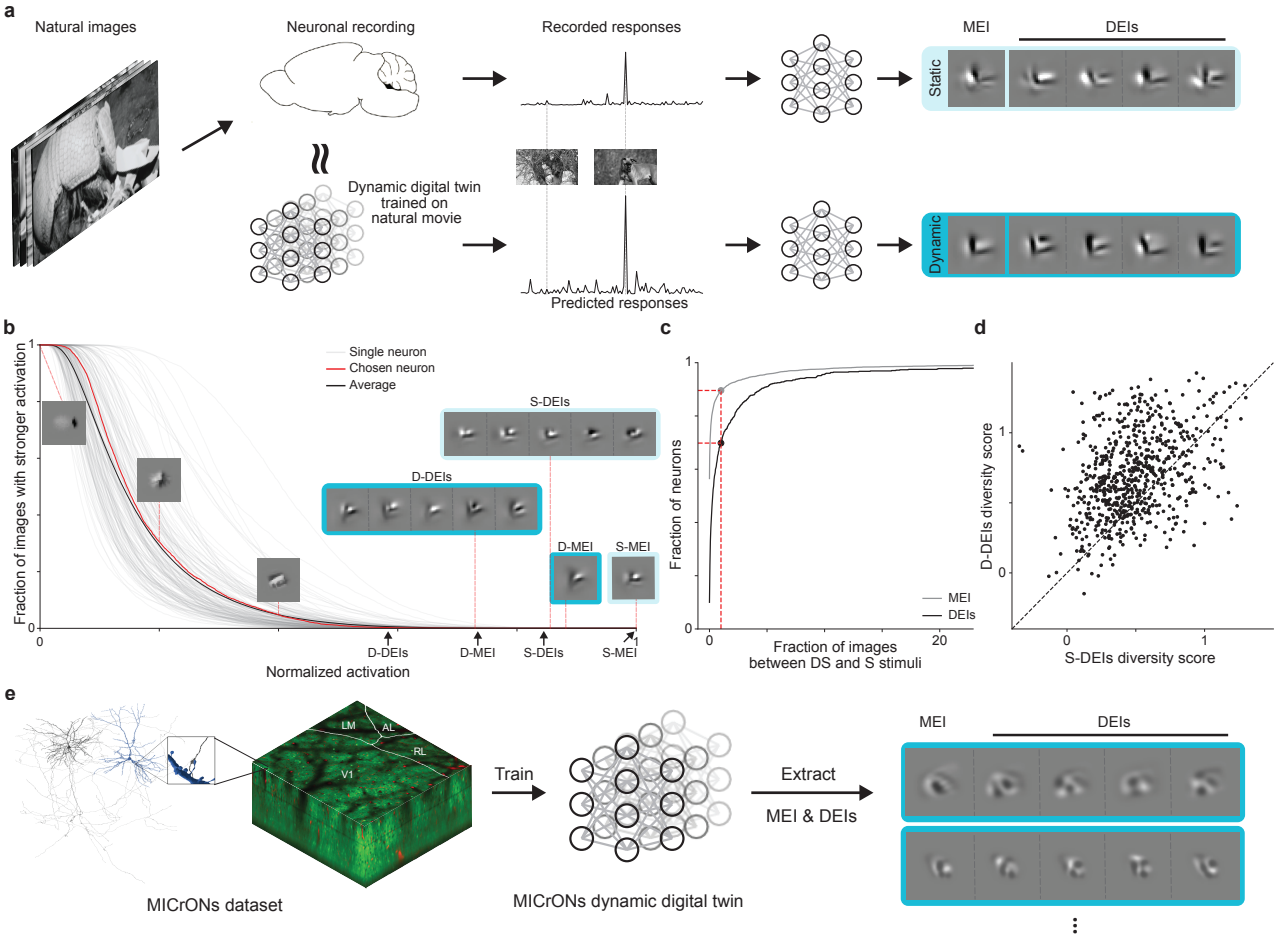

Fig. S5. Replication of DEIs in the MICrONS functional connectomics data set. **a**, Illustration of how we applied our DEI methodology in the "MICrONS" functional connectomics data set. We used neuronal responses to natural images to train a static model and optimize MEIs and DEIs ("static", S). Then, we used the responses of the same neurons to natural movie stimuli used in the MICrONS data set to first train a dynamic model and then predict responses to static images. Based on these predictions, we trained a separate static model and optimized MEI and DEIs for the same neurons ("Dynamic", D). **b**, Neuron responses to natural image crops were sparse and smaller than those to MEI and DEIs synthesized from both static and dynamic static models. The gray curves show the fraction of natural image crops that elicit no less than certain normalized activation (normalized by S-MEI activation) for 150 random model neurons; the black curve indicates the average. Arrows denote the average activation of each stimulus type on the x axis. On average, only 1.0% of all 5000 natural crops produced *in silico* responses above D-DEIs. There existed only 0.1% of natural crops in between D-MEI and S-MEI activation and only 1.0% in between D-DEIs and S-DEIs activation. For a representative cell (red), example images at different activation levels were shown, along with its S-MEI, D-MEI, S-DEIs, and D-DEIs. Data were pooled over 3 mice for a total of 935 neurons. **c**, Cumulative distribution of neurons with an equal or larger fraction of natural images crops eliciting activation in between D-MEI and S-MEI activation (gray) and in between D-DEIs and S-DEIs activation (black) (90% and 70% of all neurons have only 1% of natural patches in between D-MEI and S-MEI activation and in between D-DEIs and S-DEIs activation, respectively (red dashed line)). **d**, Diversity index of D-DEIs versus S-DEIs. Data was pooled over 3 mice for a total of 4268 neurons for MEI and 679 for DEI analysis. **e**, We used the above pipeline to optimize MEIs and DEIs for neurons in the MICrONS data set itself. This allows future circuit-level dissections towards understanding the mechanism underlying the novel bipartite invariances in mouse visual cortex.

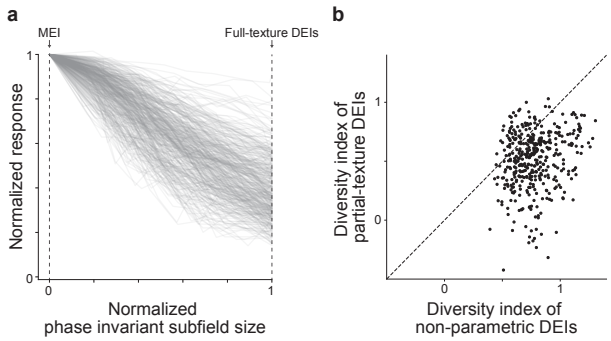

Fig. S6. Selection and quantification of partial-texture DEIs. **a**, Each curve shows how the normalized average *in silico* activation of texture-based DEIs decreases as the normalized size of phase invariant subfield increases. Texture DEIs with no phase invariant subfield (i.e. fixed subfield only) are equivalent to the MEI. Texture DEIs with phase invariant subfield spanning the entire RF is equivalent to full-texture DEIs. The set of partial-texture DEIs is selected for each neuron to jointly maximize both the average response and diversity (see Method for more details). **b**, Diversity index of partial-texture DEIs versus non-parametric DEIs. Data were shown for a total of 401 neurons pooled over 8 mice that have been tested in closed-loop experiments.

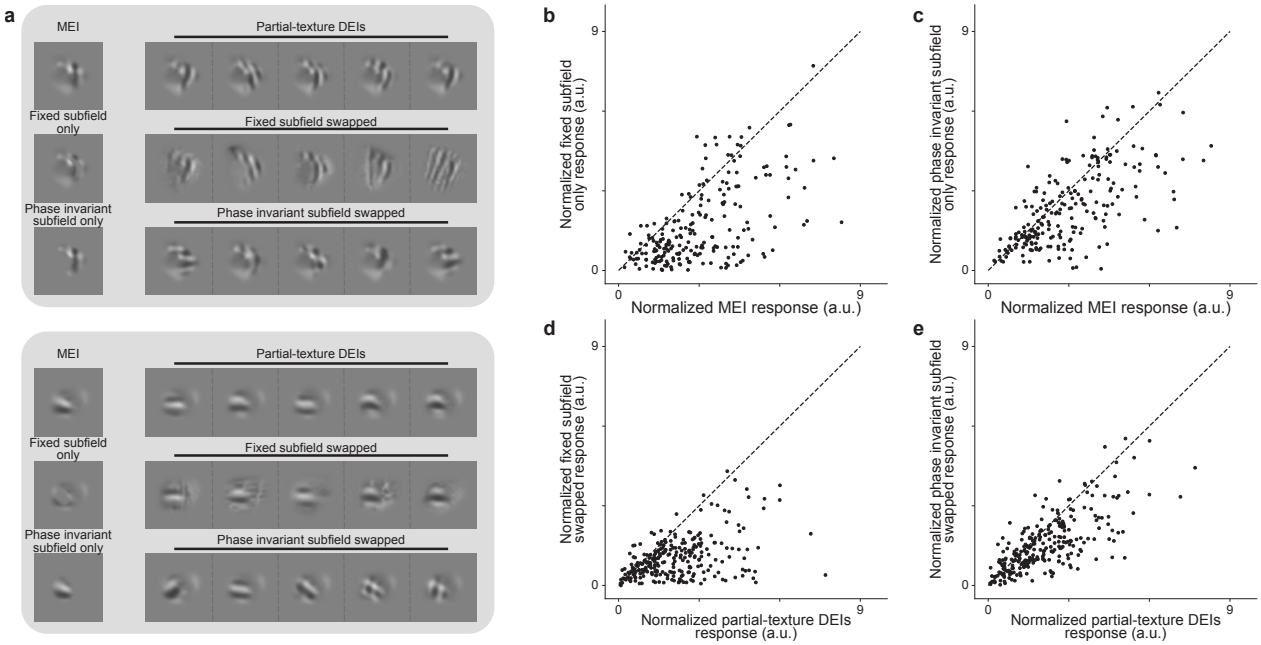

Fig. S7. Both subfields of the partial-texture DEIs are necessary and specific for evoking high *in vivo* responses. **a**, Examples of the MEI, fixed or phase invariant subfield of the MEI only, partial-texture DEIs, and partial-texture images with either fixed or phase invariant subfield swapped to random content for two example neurons. The fixed subfield was swapped to 20 different random natural patches whereas the phase invariant subfield was swapped to patches cropped from 20 different random non-self neurons' preferred textures for the phase invariant subfield. **b-e**, Each point corresponds to the normalized response of a single neuron averaged over 20 repeats (MEI) or averaged over 20 single-trial different stimuli of the same type. **b**-**c**, Fixed or phase invariant subfield of the MEI only activated the target neurons weaker than the MEI (one-sided Wilcoxon signed-rank test, $W = 21650$, $P < 10^{-9}$, and $W = 17873$, $P < 10^{-9}$, respectively) with 50.2% and 21.4% of all neurons showing weaker responses than their MEIs ($P < 0.05$, one-tailed Welch's t-test with 29.9 and 33.1 average d.f., respectively). **d**-**e**. Both fixed and phase invariant subfield swapped stimuli activated the target neurons weaker than partial-texture DEIs (one-sided Wilcoxon signed-rank test, $W = 31710$, $P < 10^{-9}$, and $W = 27850$, $P < 10^{-9}$, respectively) with 40.9% and 22.0% of all neurons showing weaker responses than their partial-texture DEIs ($P < 0.05$, one-tailed Welch's t-test with 30.0 and 32.5 average d.f., respectively). Data were pooled over 5 mice, displaying a total of 259 neurons.

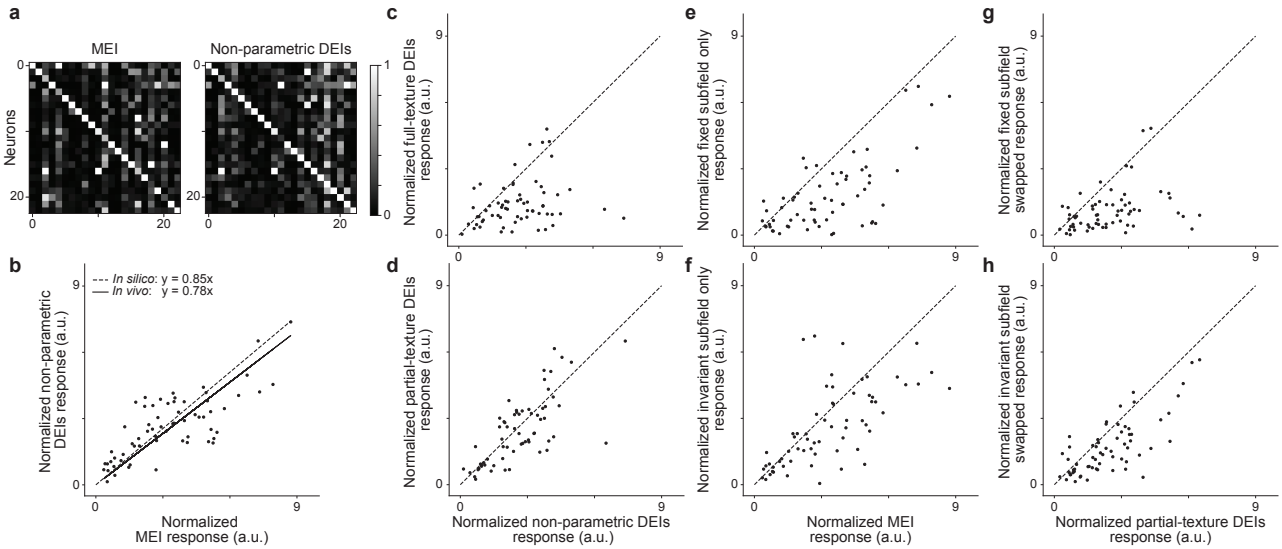

Fig. S8. DEI closed-loop verification for randomly selected neurons. **a**, Confusion matrices for MEI and non-parametric DEIs show the responses of each neuron to the MEI (left) and DEIs (right) of all target neurons. The responses of each neuron were normalized, and each row was scaled so the maximum response across all images equals 1. Responses of neurons to their own MEI and DEIs (along the diagonal) were larger than to other MEIs and DEIs respectively (one-sided permutation test, $P < 10^{-9}$ for both cases). **b-h**, Each point corresponds to the normalized response of a single neuron averaged over 20 repeats (MEI) or averaged over 20 single-trial different stimuli of the same type. **b**, *In vivo* response to DEIs versus MEI. Each point corresponds to the normalized response of a single neuron. The linear relationship between DEIs and MEI responses was estimated by averaging over 1000 repeats of robust linear regression using the RANSAC algorithm (21). DEIs stimulated neurons *in vivo* closely to the level predicted *in silico* with respect to MEI (78% versus 85%) (two-sided Wilcoxon signed-rank test, $W = 982$, $P = 0.698$), with only 14% neurons showing different responses between DEIs and 85% of MEI ($P < 0.05$, two-tailed Welch's t-test with 33.0 average d.f.). **c**, $\text{DEIs}_{\text{full}}$ failed to stimulate their target neurons compared to non-parametric DEIs (one-sided Wilcoxon signed-rank test, $W = 212$, $P = 1.53 \times 10^{-8}$) with 48.4% of all neurons showing weaker responses than non-parametric DEIs ($P < 0.05$, one-tailed Welch's t-test with 30.5 average d.f.) **d**, $\text{DEIs}_{\text{partial}}$ activated their target neurons similarly to non-parametric DEIs (two-sided Wilcoxon signed-rank test, $W = 851$, $P = 0.21$) with only 9.4% of neurons showing different responses from corresponding non-parametric DEIs ($P < 0.05$, two-tailed Welch's t-test with 34.4 average d.f.). **e-f**, Fixed or phase invariant subfield of the MEI only activated the target neurons weaker than the MEI (one-sided Wilcoxon signed-rank test, $W = 1950$, $P < 10^{-9}$, and $W = 1586$, $P = 1.3 \times 10^{-4}$, respectively) with 48.4% and 22.8% of neurons showing weaker responses than their corresponding MEIs ($P < 0.05$, one-tailed Welch's t-test with 31.0 and 33.4 average d.f., respectively). **g-h**. Both fixed and phase invariant subfield swapped stimuli activated the target neurons weaker than partial-texture DEIs (one-sided Wilcoxon signed-rank test, $W = 1942$, $P < 10^{-9}$, and $W = 1824$, $P = 7.9 \times 10^{-8}$, respectively) with 48.4% and 20.3% neurons showing weaker responses than their partial-texture DEIs ($P < 0.05$, one-tailed Welch's t-test with 28.1 and 31.7 average d.f., respectively). Data were collected from 1 mouse, displaying a total of 64 neurons.

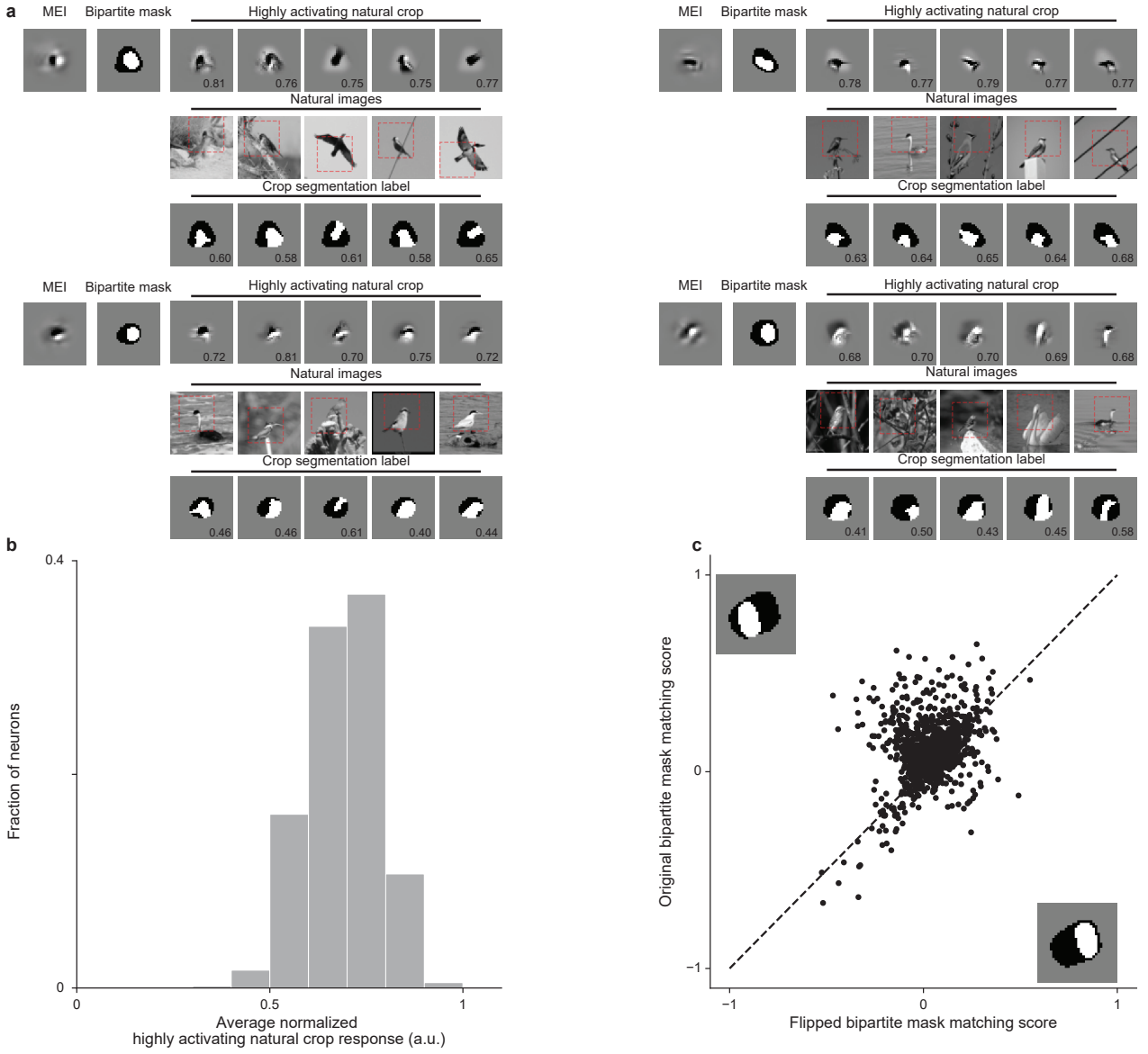

Fig. S9. DEI bipartite masks align with object boundaries in highly activating natural crops. **a**, For each of the 4 example neurons, we show the MEI, the bipartite mask (black denotes the fixed subfield and white denotes the phase invariant subfield) extracted from partial-texture DEIs, 5 of the 100 highly activating natural crops, the corresponding original full-field natural images from which the crops were taken, and the corresponding segmentation labels of the natural crops. For each highly activating crop, a matching score is computed based on its segmentation label and the neuron's bipartite mask. The value on the bottom right of each natural image crop shows the normalized model predicted activation of the image. Red dashed boxes on the full-field natural images indicate the natural image crops where the MEI masks were applied. The value on the bottom right of each segmentation label image shows its matching score. **b**, Histogram of averaged *in silico* response of top 100 highly activating natural crop sampled from CUB data set after normalized by their corresponding MEI (median is 0.695). **c**, When the bipartite mask was flipped with regard to the center of the RF, the matching score for the highly activating natural crops decreased (one-sided Wilcoxon signed-rank test $W = 204486$, $P < 10^{-9}$) with 41.3% of all neurons showing weaker matching scores than original bipartite mask ($P < 0.05$, one-tailed Welch's t-test with 186.4 average d.f.). Example original bipartite mask and flipped bipartite mask were shown for one neuron (top left and bottom right respectively). The result was pooled over 6 mice for a total of 1200 neurons.

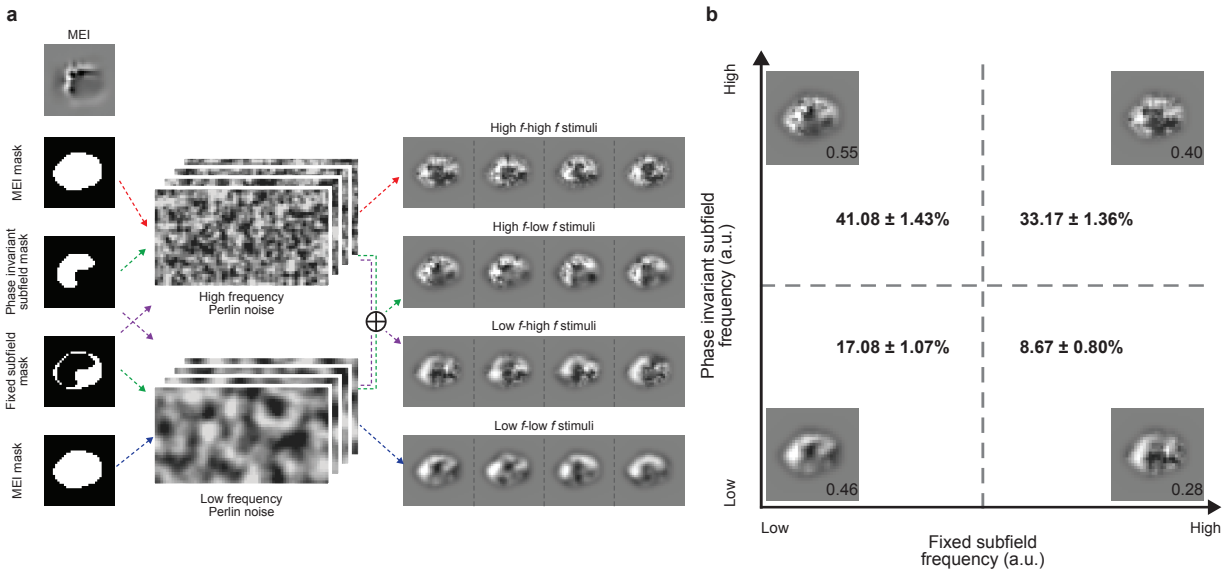

Fig. S10. Phase invariant subfields prefer higher frequency content than fixed subfields. a, Schematic illustrating the synthesis of Perlin noise stimuli (27) with different frequency biases. The MEI, bipartite mask, and synthesized stimuli for one example neuron were shown for demonstration. Two populations of full-field textures containing Perlin noise with different persistence coefficients (1.0 and 0.25) were synthesized (1 million each) to capture the diversity of natural textures at high and low frequencies (top and bottom). For each target neuron, the MEI mask was applied onto either high-frequency or low-frequency textures to create homogeneous stimuli (1 million high *f*-high *f* and 1 million low *f*-low *f*, respectively). In addition, the phase invariant subfield mask and the fixed subfield mask were applied onto different texture populations to create heterogeneous stimuli (1 million high *f*-low *f* and 1 million low *f*-high *f*). **b**, For each neuron, we screened through all 4 million synthesized stimuli to identify the most exciting one. The percentage of neurons preferring each stimulus type is reported in the 4 quadrants of the stimulus space. Each quadrant also demonstrates one example stimulus created for one example neuron, with the value on the bottom right of each image showing its normalized model predicted activation. Neurons preferred stimuli with higher frequency in the phase invariant subfield more than stimuli with low or high frequency in both subfields, as well as stimuli with lower frequency in the phase invariant subfield (one-way chi-squared test, $\chi^2 = 314$, $P < 10^{-9}$ and one-sided test using bootstrapping, $P < 10^{-9}$ for all three comparisons). The percentages of neurons for each quadrant with bootstrapped standard deviation were reported. Data was pooled over 6 mice for a total of 1200 neurons.